JOURNAL OF Applied Polymer SCIENCE

Nucleation Effect of Surface Treated TiO_2 on PTT (Polytrimethylene Terephthalate) Nanocomposites

V. Ramesh, S. Mohanty, B. P. Panda, S. K. Nayak

Laboratory for Advanced Research in Polymeric Materials (LARPM), Central Institute of Plastics Engineering and Technology (CIPET), Bhubaneswar, India

Correspondence to: S. K. Nayak (E-mail: drsknayak@gmail.com)

ABSTRACT: A study of the nucleation effect of TiO_2 in poly(trimethylene terephthalate)/TiO_2 nanocomposite has been carried out using different theoretical models. The models were applied and developed with the aim to describe and better understand the influence of the TiO_2 dispersion on crystallization characteristics of PTT. The PTT/TiO_2 nanocomposites with untreated and surface-treated TiO_2 were prepared by the melt mixing method. The nucleation efficiency of the TiO_2 nanoparticles has been analyzed with the use of the Avrami model and Mo's method. It was found that the PTT matrix incorporated with surface-treated TiO_2 particles has a higher crystallization temperature and melting point than that incorporated with untreated TiO_2 particles. As per the models, unlike untreated TiO_2, surface-treated TiO_2 particles had a lesser effect on the degree of crystallization of the PTT matrix. The TiO_2 nanoparticles act as a nucleating agent in the PTT matrix thereby reducing $t_{1/2}$ of the crystallization and leading to easier crystallization of the polymer. © 2012 Wiley Periodicals, Inc. J. Appl. Polym. Sci. 000: 000–000, 2012

KEYWORDS: PTT; nonisothermal crystallization kinetics; nano-TiO_2; surface modification

Received 1 June 2011; accepted 13 February 2012; published online
DOI: 10.1002/app.37562

INTRODUCTION

Poly(trimethylene terephthalate) (PTT) was first patented by Whinfield and Dickson in 1941. PTT, a thermoplastic aromatic polyester, has been a potential competitor of PBT and PET in packaging, textiles, and other high end applications. PTT material possesses several advanced properties such as enhanced tensile and flexural strength, high elastic recovery chemical resistance and resilience, thermal and barrier properties that makes the material most competitive among its counterparts.[1–6] The polymer has typical semicrystalline characteristics, and the investigation of its crystallization kinetics has been a significant importance in both scientific and technological points of view. PTT crystallizes faster than PET but slower than PBT,[7] hence many properties of PTT such as crystallization rate and glass transition temperature lies in between of PET and PBT. Several important findings[8–13] about PTT have been published recently; primarily to using on the study of crystallization kinetics,[12] crystal structure,[10] and melting behavior[12] of PTT. However, investigations pertaining improvement of the properties of PTT have been still under progress.[14]

Compounding of polymers with nanoscale level fillers to improve the properties have generated considerable research interests in the recent years.[15] Improved mechanical strength, enhanced modulus, decreased thermal expansion coefficient, increased thermal stability, and reduced gas permeability compared with pure polymers by addition of small fraction of nanoclay to the tune of 3–5 wt % have been reported by various workers.[6] Combination of properties of the inorganic nanoparticles in particular rigidity and thermal stability, with the inherent properties of the polymer such as toughness and easy processability to produce nanocomposites with excellent properties have been a primary objective to obtain products with desired attributes.[16] TiO_2 nanoparticles are widely used as fillers in plastics. These fillers may act as a nucleating agents or antinucleating agents and thus effect the over crystallization behavior of the matrix polymer.[17,18] However, its uniform dispersion within the polymer matrix has been a difficult task because of its incompatibility with the latter. Surface treatment of the nanoparticles is one of the effective methods to enhance the miscibility with the polymer matrix.[19] Therefore, understanding the parameters affecting crystallization has been crucial for the optimization of the processing conditions and the properties of the end product.[20,21] Extensive investigations of Zhu et al.[22] on PET/TiO_2 nanocomposites have shown that the TiO_2 nanoparticles act as an antinucleating agent in the PET matrix.

In this article, studies on PTT/TiO_2 and surface-treated TiO_2 nanocomposites under nonisothermal conditions has been

evaluated using differential scanning calorimetry (DSC). The effect of TiO_2 on the crystallization kinetics of PTT has been analyzed based on the Avrami's method, and Mo's method, respectively. The activation energies were calculated according to the Kissinger model. SEM studies have been used to evaluate the miscibility characteristics of TiO_2 with the PTT and its compatibility in the nanocomposites.

EXPERIMENTAL METHODS

Materials

Poly(trimethylene terephthalate); PTT (Grade: Futura CPTT® 495-09) was kindly supplied by M/s Futura polymers Ltd. Chennai, (India). The melting point of PTT used was 231.4°C, with an intrinsic viscosity 0.928 dL/g. The TiO_2 nanoparticles of anatase type (Grade: Nanoshel® Ti-Nano N-1102) were supplied by M/s Nanoshel LLC (USA) having a diameter of about 40–60 nm. γ-Aminopropyltriethoxysilane was supplied by Evo n/k Degussa GmbH Inorganic Materials (Germany). Dimethy sulphoxide (DMSO) was obtained from M/s Merck Specialities Pvt. Ltd. Mumbai. 3-Glycidoxypropyltrimethoxysilane (GPS) (98%), methyl Methacryalte (MMA) 99%, 2-methylpyridine (Picoline 98%), and 4,4′-azobis(4-cyanovaleric acid) (ACVA) (97%) were purchased from M/s Sigma-Aldrich, USA. All other solvents of AR grade were used as received.

Surface-Treatment of TiO_2 Nanoparticles

GPS-Grafted TiO_2. The preparation of surface-treated TiO_2 nanoparticles is shown in Scheme 1. A total of 0.5 mL of GPS was dissolved in 100 mL methylbenzene solution, and the pH level of the solution was maintained between 2 and 4. The solution was kept at room temperature for 2 h under medium stirring condition to initiate hydrolysis reactions. Subsequently, 10 g of TiO_2 nanoparticles was added into the solution under constant sonication for 15 min, and the resulting suspension was refluxed at 70–90°C for 8 h. Finally, the suspension was filtered and washed thoroughly by Soxhlet's extraction for 12 h, and GPS-grafted TiO_2 nanoparticles were obtained after vacuum drying at 60°C in 9 h.

PMMA-Grafted TiO_2. PMMA-grafted TiO_2 was prepared using a two-step procedure. In the first step, GPS-grafted TiO_2 particles were treated with ACVA to prepare ACVA-GPS-grafted TiO_2 using the following process. A total of 3 g of GPS-grafted TiO_2 nanoparticles was dispersed in 50 mL DMSO with 1 wt % of ACVA and 1 wt % of 2-methylpyridine under nitrogen flow by sonication. The suspension was heated to 50°C with high magnetic stirring for 5 h. Then, the suspension was filtered, washed with excess of methanol several times, to remove the smell of picoline, and finally vacuum-dried for 4 h at 40°C to obtain the ACVA-GPS-grafted TiO_2 particles.

Subsequently, in the second step, 0.3 g ACVA-GPS-grafted TiO_2 particles was dispersed in 25 mL MMA under constant nitrogen flow by sonication. The suspension was heated to 70°C with vigorous stirring for 2 h. The suspension was filtered, washed with excess of methanol several times, and vacuum-dried for 2 h at 40°C to obtain PMMA-grafted TiO_2.

γ-Aminopropyltriethoxysilane-Grafted TiO_2. A total of 0.5 mL of γ-aminopropyltriethoxysilane was dissolved in 40 mL of water and the pH maintained in between 2 and 4. The mixture

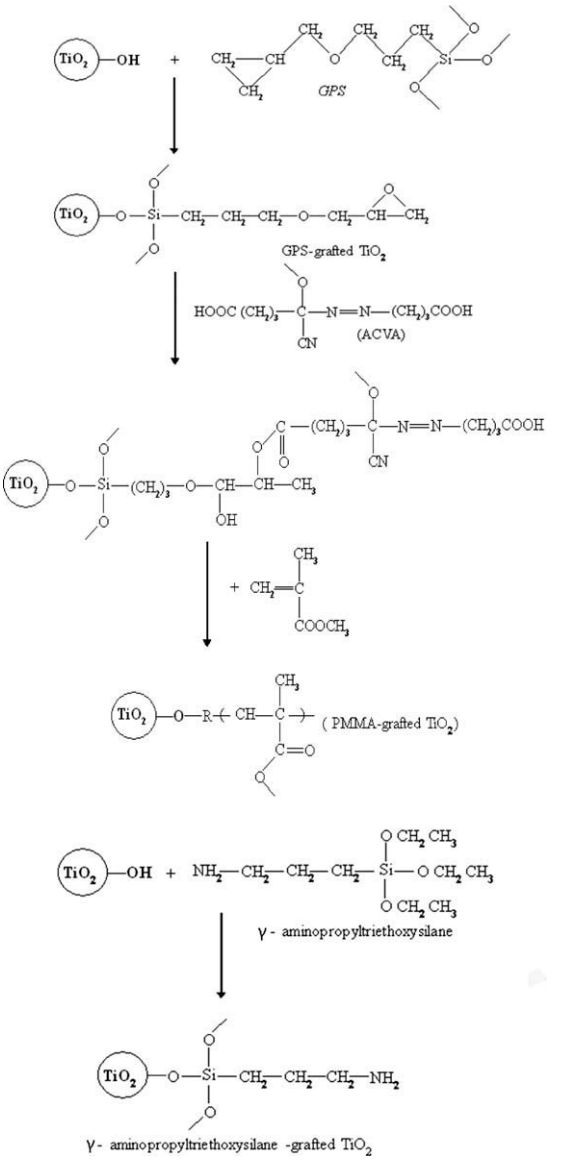

Scheme 1. Preparation of surface-treated TiO_2 nanoparticles.

was kept at room temperature for 2 h under high magnetic stirring to initiate hydrolysis reactions. A fine dispersion of 2 g of TiO_2 nanoparticles into 50 mL of ethanol was then added to this solution and was kept for 15 min under sonication. Then, the solution is kept at 70°C for 24 h under constant magnetic stirring. After the reaction, the treated TiO_2 nanoparticles have been dried at 80°C. The reaction mechanism have been given in Scheme 1.

Preparation of PTT/TiO_2 Nanocomposite

In this work, PTT/TiO_2 nanocomposite was prepared at different compositions of PTT/TiO_2 (99.5/0.5, 99/01, 98.5/1.5, 98/02, and 97/03) using Rheomix 600 (Germany), batch mixer with counter rotating blades of 69 cm^3 volumetric capacity. Before compounding, the virgin material was dried at 110°C in vacuum oven for 24 h. The TiO_2 nanoparticles were also predried at 80°C in vacuum oven for 4 h. PTT and TiO_2 nanoparticles were mixed at the temperature of 230–240°C and screw speed

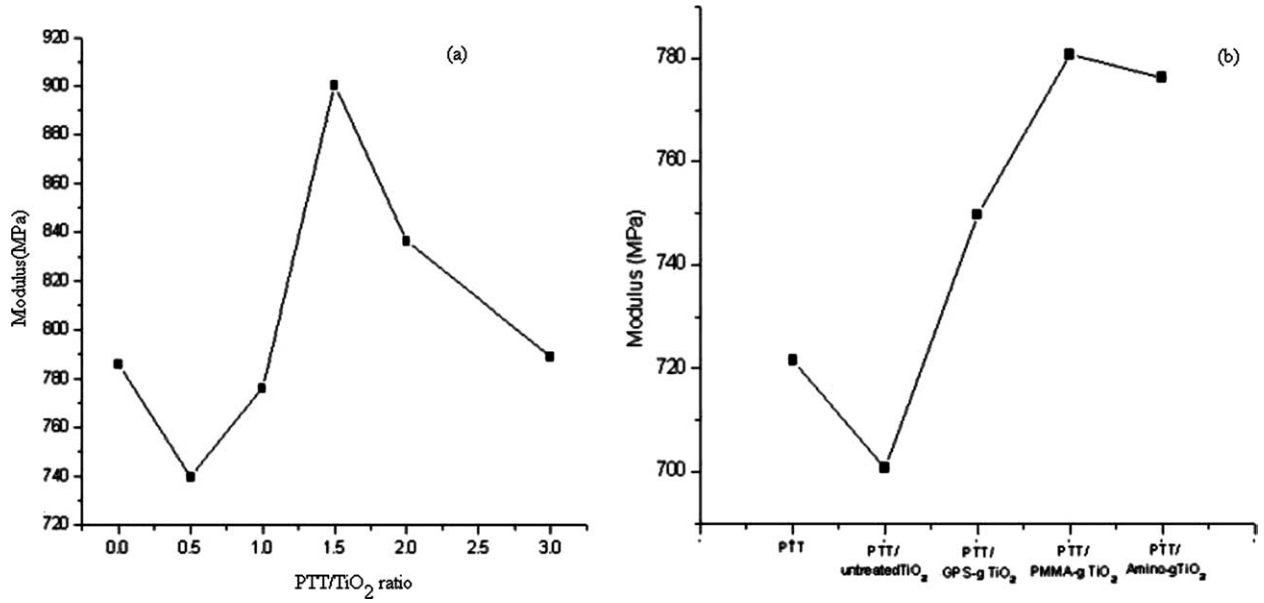

Figure 1. Mechanical properties.

of 45–50 rpm for 5 min. Subsequently, the most mixes were brought to room temperature and compression moulded at 240°C 15 min cycle time with 60–70 MPa pressure and cooling time of 35 min using a compress press (M/s Dalta Malikson Mumbai, India) Then, the specimens were prepared as per standard ASTM D 638, type V model.

Minimum six samples of each are tested in mechanical testing. The average result of mechanical testing values that was optimized was 98.5/1.5 composition ratio.

The influence of TiO_2 nanoparticles on the mechanical properties of PTT is given in Figure 1, respectively. It is observed that the modulus values decrease slightly in the presence of 0.5 wt % of TiO_2 in the nanocomposites. Then slowly it increases in the peak of 98.5/1.5 ratio of PTT/TiO_2 nanocomposites, beyond which at higher concentration of TiO_2, the tensile strength and modulus decreases drastically. This reveals agglomeration and micro crack formation at higher concentration of TiO_2. Because PTT/TiO_2 nanocomposite at a ratio of 98.5/1.5 shows optimum modulus and strength, this composition has been optimized and taken for further studies.

Characterization

Tensile strength was measured according to ASTM D 638 type V, at a crosshead speed of 10 mm/min using a Universal Testing Machine (UTM), (M/s INSTRON, UK) testing machine. All the values reported are an average of six samples measurements. The nonisothermal analyses of the nanocomposites samples were carried out using a (TA Instrument USA) DSC. The temperature was calibrated using a standard reference Indium. All DSC measurements were performed under nitrogen atmosphere and a sample of weight 5–10 mg was taken. All samples were heated from 40 to 300°C at the heating rate of 20°C and then hold at 300°C for 5 min to eliminate the previous thermal history. Subsequently, the samples were cooled to 120°C at a cooling rate 5, 10, 15, and 20°C/min, respectively, and the exothermic crystallization peak was recorded as a function of temperature. The existence of the interfacial bonds in the surface-treated TiO_2 nanoparticles was examined using FTIR microscopy (M/s Nicolet 6700, USA). A resolution of 60 scan per minute and wavelength range of 1000–3400 cm^{-1} was used. The scanning electron microscopy (SEM, EVO 15, Carl Zeiss, Germany) of the tensile fractured surface of the nanocomposites samples were taken to investigate the internal morphology. The samples were sputter coated before taking image.

RESULTS AND DISCUSSION

Mechanical Properties

Figure 1(b) depicts the variation of tensile modulus of virgin PTT and its nanocomposites. It is evident that the tensile modulus increases in case of treated PTT/TiO_2 nanocomposites thus

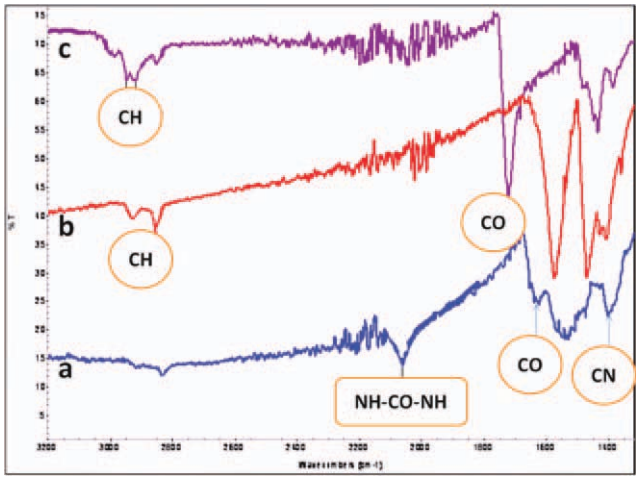

Figure 2. FTIR spectra of (a) amino-grafted TiO_2, (b) GPS-grafted TiO_2, and (c) PMMA-grafted TiO_2. [Color figure can be viewed in the online issue, which is available at wileyonlinelibrary.com.]

Applied Polymer SCIENCE

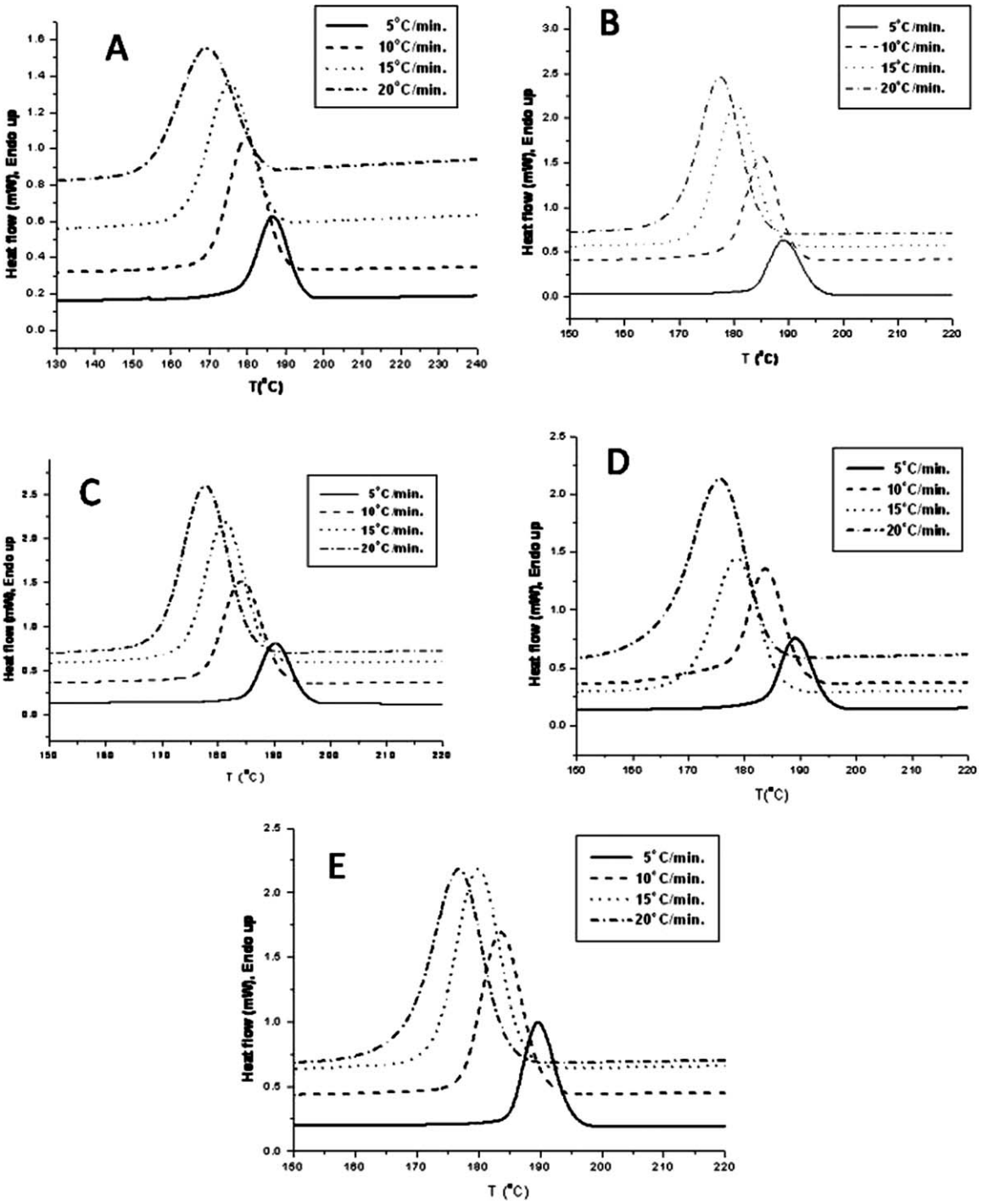

Figure 3. DSC thermograms of nonisothermal crystallization for (A) Pure PTT, (B) PTT/TiO_2, (C) PTT/GPS-grafted TiO_2, (D) PTT/PMMA-grafted TiO_2, (E) PTT/amino-grafted TiO_2.

revealing improved interfacial adhesion between the treated TiO_2 and PTT matrix. PTT/GPS-grafted TiO_2 shows a higher modulus value of 749.73 MPa which is nearly 6.54% higher than PTT/untreated TiO_2, suggesting incompatibility of the untreated TiO_2 nanoparticles with the PTT matrix. The value of PTT/ GPS-grafted TiO_2 is probably due to hydrogen bonding interaction between the silane oxygen with the PTT matrix. PTT/PMMA-grafted TiO_2 nanocomposite exhibited an optimum tensile modulus of 780.73 MPa. This behavior is primarily attributed to covalent linkage between PMMA with TiO_2 which again interlinks with the PTT matrix through vander waals forces of interaction. Similar facts have been reported by Wang et al.,[23] where in the modification of TiO_2 using silane coupling agent is crucial to ensure the covalent bond bindings between

Table I. Nonisothermal Crystallization Kinetic Parameter Values of T_i, T_p, and $T_{1/2}$

	φ (°C/min)	T_i (°C)	T_p (°C)	$\tau_{1/2}$ (s)
PTT	5	197.89	186.42	140
	10	193.21	179.81	82
	15	190.36	175.28	60
	20	187.39	171.57	48
PTT/TiO_2	5	198.86	188.82	116.4
	10	194.79	182.91	72.79
	15	192.34	179.74	52.39
	20	189.35	177.75	37.4
PTT/GPS-grafted TiO_2	5	198.53	190.09	103.2
	10	194.94	184.27	66.4
	15	192.82	181.16	48.39
	20	190.62	178.42	38.2
PTT/PMMA-grafted TiO_2	5	197.37	189.02	102.59
	10	193.76	182.66	68.59
	15	189.15	178.68	44.2
	20	185.56	175.59	55.4
PTT/Amino-grafted TiO_2	5	199.3	189.59	118.8
	10	195.58	183.68	74
	15	192.37	179.94	51.8
	20	188.68	176.81	37.4

the PMMA chain with TiO_2 particles during the preparation of PTT/poly(methyl methacrylate)-grafted TiO_2 nanocomposite. A PTT/γ aminopropyltriethoxysilane-grafted TiO_2 nanocomposite also exhibited a higher tensile modulus of 776.31 MPa, about 9.74% higher than the untreated nanocomposites thus confirming strong covalent bond between the PTT martris and amino group. Hence comparing the modulus data of all the samples, the results depict the following order, PTT/TiO_2 > PTT > PTT/GPS-grafted TiO_2 > PTT/PMMA-grafted TiO_2 ≥ PTT/γ amino-grafted TiO_2.

FTIR Analysis

To illustrate the structural changes before and after treatment of TiO_2, the FTIR spectra of treated TiO_2 were recorded in the range of 400–4000 cm^{-1}. Figure 2 shows the FTIR spectra of amino propyltriethoxysilane-grafted TiO_2, GPS-grafted TiO_2, and PMMA-grafted TiO_2. The FTIR spectra of amino propyltriethoxysilane-treated TiO_2 [Figure 2(a)] showed characteristic carbonyl stretching (CO) at 1690 cm^{-1}, NH—CO—NH urea at 2273 cm^{-1}, and nitrile group CN at 1400 cm^{-1}, respectively.[24] This indicates effective interfacial linkage of amino nanoparticles on to TiO_2. In [Figure 2(b)], the peaks at 2927.3 cm^{-1} and 2852.2 cm^{-1} corresponds to the stretching of cyclic and linear methyl group of GPS, which indicates that GPS chains have been grafted at the TiO_2 surface.[25] Similarly, [Figure 2(c)] displayed bands at 1721.2 cm^{-1} due to stretching vibrations of C=O groups which belongs to PMMA-grafted TiO_2 surface in the process of polymerization.[26] This further confirms the modification PMMA are treated with the TiO_2 nanoparticles.

Nonisothermal Crystallization Kinetics

The study of nonisothermal crystallization is of greater practical importance because the nonisothermal conditions are closer to real industrial processing conditions.[26] The DSC thermograms of nonisothermal crystallization for PTT, PTT/TiO_2, PTT/GPS-grafted TiO_2, PTT/PMMA-grafted TiO_2, and PTT/amino-grafted TiO_2 at different cooling rates (5, 10, 15, and 20°C) are presented in Figure 3. The parameters of crystallization data are listed in Table I. It can be seen that the crystallization peak temperature (T_p) and the initial crystallization temperature (T_i) for the PTT/surface-treated TiO_2 nanocomposite are lower than those of PTT at the same cooling range. This indicates that the existence of TiO_2 nanoparticles makes the crystallization of nanocomposite become easier when compared with pure PTT.

Table I represents a comparative data of PTT nanocomposites at various cooling rates. Figure 4 shows the shift of the crystallization temperature and heat flow changes, which is an effect of addition of surface-treated TiO_2 nanoparticles in PTT matrix. The $t_{1/2}$ (half time of crystallization) is also listed in Table I. It is evident that $t_{1/2}$ decreases with increasing cooling rate, which indicates faster crystallization rate as the cooling rate increases.[27] Comparing the $t_{1/2}$ of pure PTT with that of TiO_2-incorporated nanocomposites, the crystallization rate of PTT was increased by the addition of TiO_2 nanoparticles. This is probably due to fact that the TiO_2 nanoparticles act as nucleating agents during deformation of a sample by preventing the formation of the crystalline nodes that eventually develop into three-dimensional network structures.[26] The relatively poor interaction between the TiO_2 nanoparticles and the polymer chains in the rubbery temperature could be also responsible to suppress the crystallization process. However, comparing PTT/TiO_2 nanocomposites, with the GPS, PMMA, and amino-grafted TiO_2 variable surface nanocomposites a lesser reduction in crystallization rate was observed. This behavior is probably due to treatment methods which greatly affects the crystallization process of matrix. PTT/PMMA-grafted TiO_2 and PTT/amino-grafted TiO_2 nanocomposites exhibit increases in crystallization rate at all heating rate, which indicates better miscibility characteristics with the PTT matrix. Zhu et al.[22] also observed similar results wherein PMMA-grafted TiO_2 nanocomparticles showed reduction in crystallization rate and better compatibility with PET matrix.

The relationship between temperature (T) and time (t) is given by eq. (1) during the nonisothermal crystallization process is represented as follows:

$$t = \frac{|T_0 - T|}{\varphi} \tag{1}$$

where t is the crystallization time, T_o is the initial crystallization temperature ($t = 0$), T is the temperature at a crystallization time t, and φ is the cooling rate. The relative degree of crystallinity, X_t as a function of temperature can be defined as:

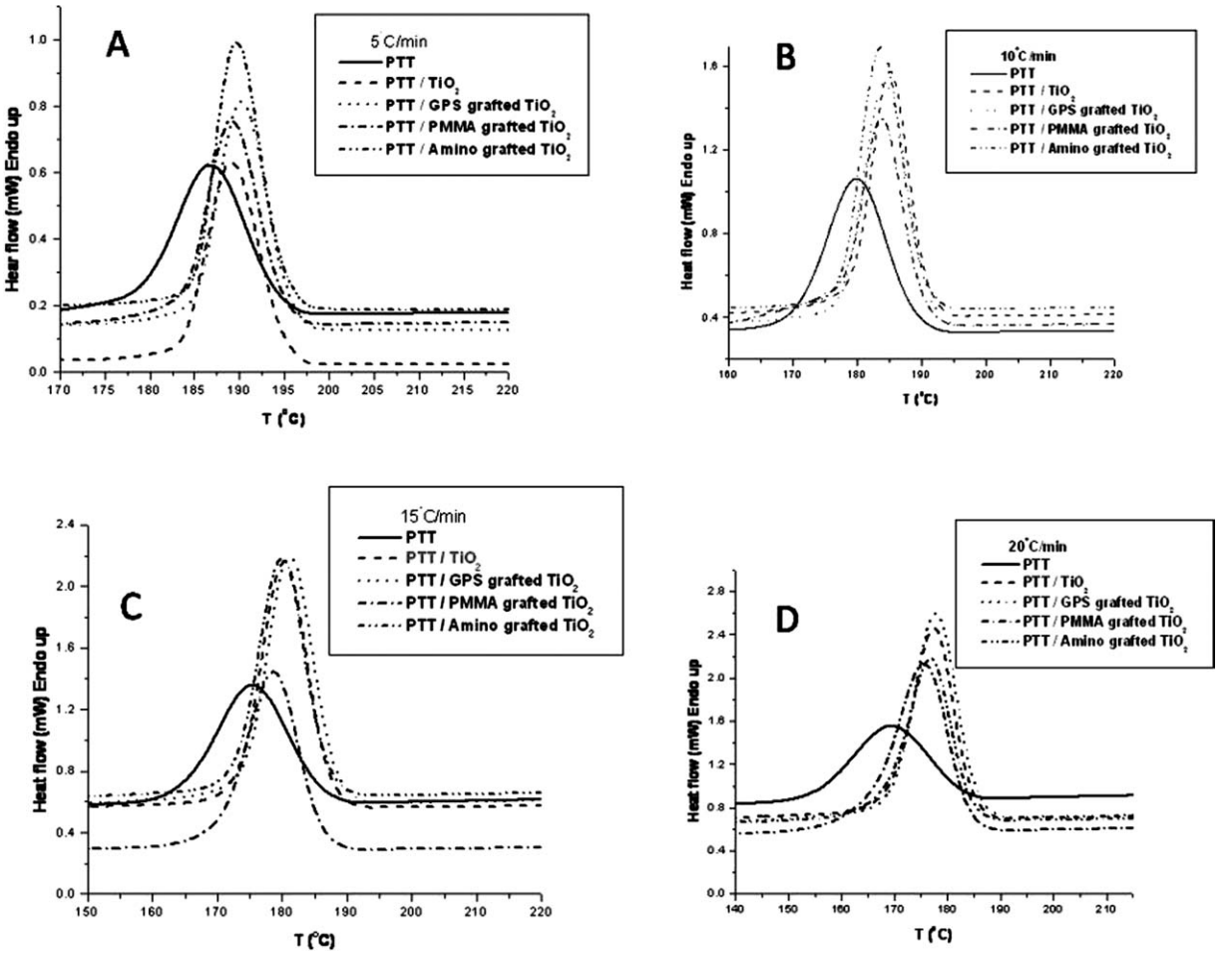

Figure 4. Same cooling rate and different composites DSC thermograms of (A) 5°C, (B) 10°C, (C) 15°C, and (D) 20°C.

$$X_t = \frac{\int_{T_0}^{T} (dH_c(T)/dT)dT}{\int_{T_0}^{T_\infty} (dH_c(T)/dT)dT} \quad (2)$$

where T_o and T_∞ are the initial and final crystallization temperature, respectively. Figure 5 shows relative crystallinity (X_t) calculated at different temperature (T) from the DSC data of the virgin matrix and the nanocomposites samples.

Avrami Theory Analysis

The crystallization kinetics of polymers is analyzed using a classical Avrami equation[28–30] as given in eq. (3)

$$1 - X_t = \exp(-kt^n) \quad (3)$$

where X_t is the development of crystallinity X_c at time t. The fraction of X_t is obtained from the area of the exothermic peak in DSC crystallization analysis at a theoretical calculation of X_t, crystallization time t divided by the total area under the exothermic peak eq. (2).

$$X_t = \frac{A_T}{A_{\text{Total}}} \quad (4)$$

$$\ln[-\ln(1 - X_t)] = \ln k + n \ln t \quad (5)$$

The k value is the Avrami rate constant and the n value is the Avrami exponent. Both value of k and n depends on the nucleation or antinucleation and growth mechanisms of spherulites. Equation (5) is double logarithmic form of eq. (3). The k and n values are obtained using eq. (5) from the slope and intercept of the fitting straight lines.[31] Figure 6 shows plots of ln t vs. ln[−ln(1 − X_t)] for nonisothermal crystallization of five samples. This plot gives good linearity in a wide crystallinity range.

From Table II, the n values of melt crystallization are nonintegral in the range between 1.9 and 3.6. Chung et al.[26] reported similar results in PTT matrix. Generally, the n values close to 3 indicates an athermal or nucleation process followed by a three-dimensional crystal growth.[31] On the other hand, the n value close to 2 may hint an athermal nucleation process followed by a two-dimensional crystal growth.[33] Our results indicate that the nucleation mechanism depends much on crystallization temperature. The nonintegral n value may also be considered because of the crystal branching or two-stage crystal growth or mixed growth nucleation mechanisms.[33,34] The experimental result also indicates that as the crystallization cooling rate increases, the k value drastically

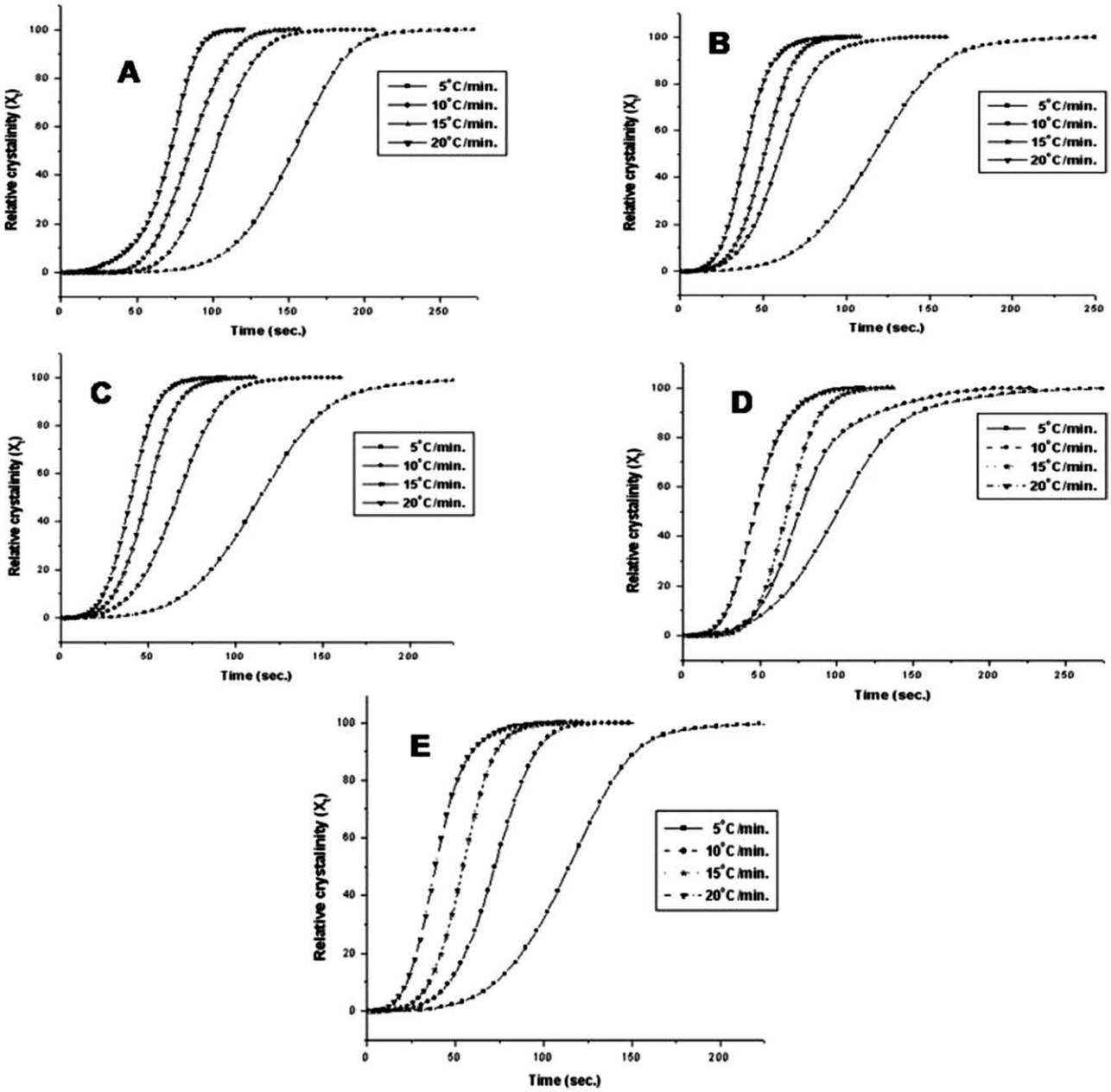

Figure 5. Relative crystallinity function of time (A) PTT, (B) PTT/TiO_2, (C) PTT/GPS-grafted TiO_2, (D) PTT/PMMA-grafted TiO_2, and (E) PTT/amino-grafted TiO_2.

increases. The k value is directly proportional to the rate of spherulites growth G. The crystallization rate is controlled by the two well-established nucleation and diffusion mechanisms, which are characterized by opposite temperature dependences.[31] By the addition of TiO_2 nanoparticles the n value changes from 1.9 to 3.6 sites. This indicates that the TiO_2 nanoparticles creates nucleation sites in the PTT matrix during the crystallization process. However, in all the treated PTT/TiO_2 nanocomposites the n is almost same, which further conforms that TiO_2 nanoparticles can effectively act as nucleating agents forming three-dimensional crystal structures. Also at higher scanning rate of 20°C/min, the n value of PTT ≈ PTT/amino-grafted TiO_2, which reveals its compatibility with the PTT matrix.

Analysis Based Mo's Method

Mo's method was also used to describe the nonisothermal crystallization for comparison. For the nonisothermal crystallization process, physical variables relating to the process are the relative degree of crystallinity X_t, cooling rate φ, and crystallization temperature T.

The Avrami equation[28] was developed for isothermal crystallization; Mandelkern et al.[35] considered that the primary stage of nonisothermal crystallization could be described by the Avrami

Applied Polymer SCIENCE

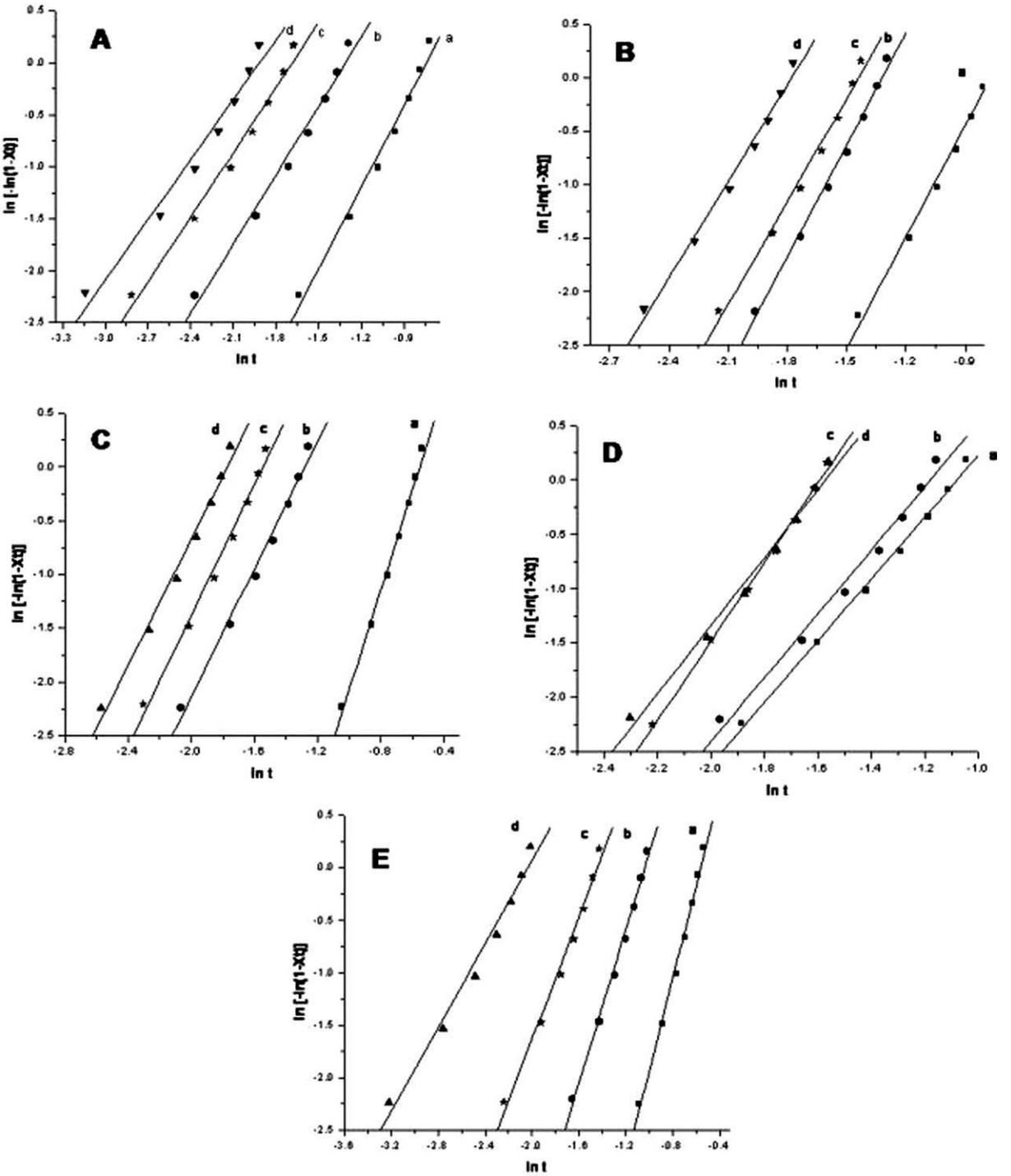

Figure 6. Plots of $\ln[-\ln(1 - X_t)]$ versus $\ln t$ for (A) PTT, (B) PTT/TiO_2, (C) PTT/GPS-grafted TiO_2, (D) PTT/PMMA-grafted TiO_2, and (E) PTT/amino-grafted TiO_2.

equation, based on the assumption that the crystallization temperature is constant, by using following equation.

$$X_t = 1 - \exp(-kt^n) \quad (6)$$

$$\log[-\ln(1 - X_t)] = \log k_t + n \log t \quad (7)$$

Both the Ozawa and Avrami equations can relate these variables as follows:

$$\log[-\ln(1 - X_t)] = \log k(T) - m \log \varphi \quad (8)$$

where $k(T)$ is a function related to the overall crystallization rate that indicates how fast crystallization proceeds and m is Ozawa exponent that depends on the dimension of crystal growth. As the crystallinity is related to the cooling rate ϕ and t can be defined for a given crystallinity.[36] Consequently,

Table II. *n* and *k* Values of Avrami Theory

	Φ (°C/min)	Ln *k*	*k*	*n*
PTT	5	1.95	7.03	2.6
	10	2.91	18.36	2.2
	15	3.51	33.51	2.1
	20	3.69	40.04	1.9
PTT/TiO_2	5	2.68	14.58	3.5
	10	3.62	37.34	3.5
	15	4.62	101.49	3.2
	20	5.34	208.51	3.0
PTT/GPS-grafted TiO_2	5	2.58	13.19	3.6
	10	3.81	45.15	2.9
	15	4.69	108.85	3.0
	20	5.21	183.09	2.9
PTT/PMMA-grafted TiO_2	5	3.06	21.33	2.8
	10	3.45	31.50	2.9
	15	4.78	119.10	3.6
	20	4.92	137.00	3.1
PTT/Amino-grafted TiO_2	5	2.46	11.70	3.4
	10	3.78	43.82	3.6
	15	4.22	68.03	2.9
	20	4.04	56.83	2.0

a new kinetic equation for nonisothermal crystallization was derived by combining eqs. (7) and (9).

$$\log k_t + n \log t = \log k(T) - m \log \varphi \tag{9}$$

and by rearrangement

$$\log \varphi = \log F(T) - \alpha \log t \tag{10}$$

where the parameters $F(T) = [k(T)/k_t]^{1/m}$ refers to the cooling rate value, which must be chosen within unit crystallization time when the measured system amounts to a certain degree of crystallinity. α is the ratio between the Avrami exponent n and Ozawa exponents m, for instance, $\alpha = n/m$ and $F(T)$ refers to the value of cooling rate chosen at unit crystallization time when the system has a certain crystallinity. Same value of $F(T)$ indicates higher rate of crystallization has been derived. Therefore, $F(T)$ has a definite physical and practical meaning.

Based on Mo's method, the plots of log φ against log t at a given crystallinity should give a straight line with an intercept of log $F(T)$ and a slope of α. Figure 7 shows a liner relationship between log ϕ and log t at a given crystallization rate for the samples, which indicates that Mo's method could be used to analyze the crystallization behavior. The values of $F(T)$ and slope α are listed in Table III. The values of α is almost the same for each sample. As the $F(T)$ values increase with the relative crystallinity, within the equal time, a quicker cooling rate (φ) was required for the same sample to get a greater relative crystallinity, which also means a larger $F(T)$ value. Therefore, if the crystallization time is the same, the relative crystallinity would increase with the cooling rates. The time needed to get the same relative crystallinity increases when PTT is filled with TiO_2 nanoparticles. This means that the presence of TiO_2 decreases the crystallization time there by increasing the crystallization rate. In other words, TiO_2 and surface-treated TiO_2 nanoparticles created nucleation three-dimensional growth in PTT/TiO_2 and PTT/surface-treated TiO_2 nanocomposites. The obtained crystallization time order from Mo's analysis is the same as from Jeziorny analysis PTT > PTT/TiO_2 > PTT/GPS-grafted TiO_2 > PTT/amino-grafted TiO_2 > PTT/PMMA-grafted TiO_2.

Crystallization Activation Energy

The method often used for evaluation of activation energy at different cooling rates was proposed by Kissinger based on the following equation.

$$\frac{d[\ln(\frac{\varphi}{T_p^2})]}{d(\frac{1}{T_p})} = -\frac{\Delta E}{R} \tag{11}$$

where R is the universal gas constant and ΔE is the activation energy of crystallization. The crystallization activation energy (ΔE) is calculated from the slope of ln (φ/T_p^2) versus $1/T_p$. Table IV and Figure 8 shows the E_a variations for TiO_2 and surface-treated TiO_2 nanocomposites when compared with the E_a of the virgin PTT. This result is quite unexpected as one can assume that the addition of TiO_2 nanoparticles into the polymer matrix favors heterogeneous nucleation and thus is expected to yield a higher E_a.[35] The PMMA-grafted TiO_2 and amino-grafted TiO_2 E_a value is almost nearer to virgin PTT. This explains that it is more miscible with PTT matrix. The other TiO_2 and GPS-grafted TiO_2 value is high, which suggests it less compatibility within the PTT polymer matrix.

SEM Analysis

Figure 9 shows that SEM images of (a) PTT/TiO_2, (b) PTT/GPS-grafted TiO_2, (c) PTT/PMMA-grafted TiO_2, and (d) PTT/amino-grafted TiO_2 nanocomposites. From Figure 9(a), it is observed that the TiO_2 nanoparticles are not distributed uniformly within the PTT matrix. The white spots are indicative of the TiO_2 nanoparticles, which may be a result of agglomerated nanoparticles. Figure 9(b) also shows evidence of nonuniform distribution of GPS-grafted TiO_2 particles on PTT matrixes. However, the dispersin in PTT/GPS-grafted TiO_2 nanocomposites is much better than PTT/TiO_2. on the contrary, Figure 9(c) shows uniform dispersion of PMMA-grafted TiO_2 in the PTT matrix. This indicates that the grafted PMMA has enhanced miscibility between TiO_2 and PTT. This may be result due to polar polar interaction which forms miscible blend. Figure 9(d) γ-aminopropyltriethoxysilane-grafted TiO_2 is dispersed uniformly in the polymeric matrix, which indicates that the grafted γ-aminopropyltriethoxysilane enhanced the miscibility between γ-aminopropyltriethoxysilane TiO_2 and PTT, because of hydrogen bonding of amino group and PTT matrix.[22]

Applied Polymer SCIENCE

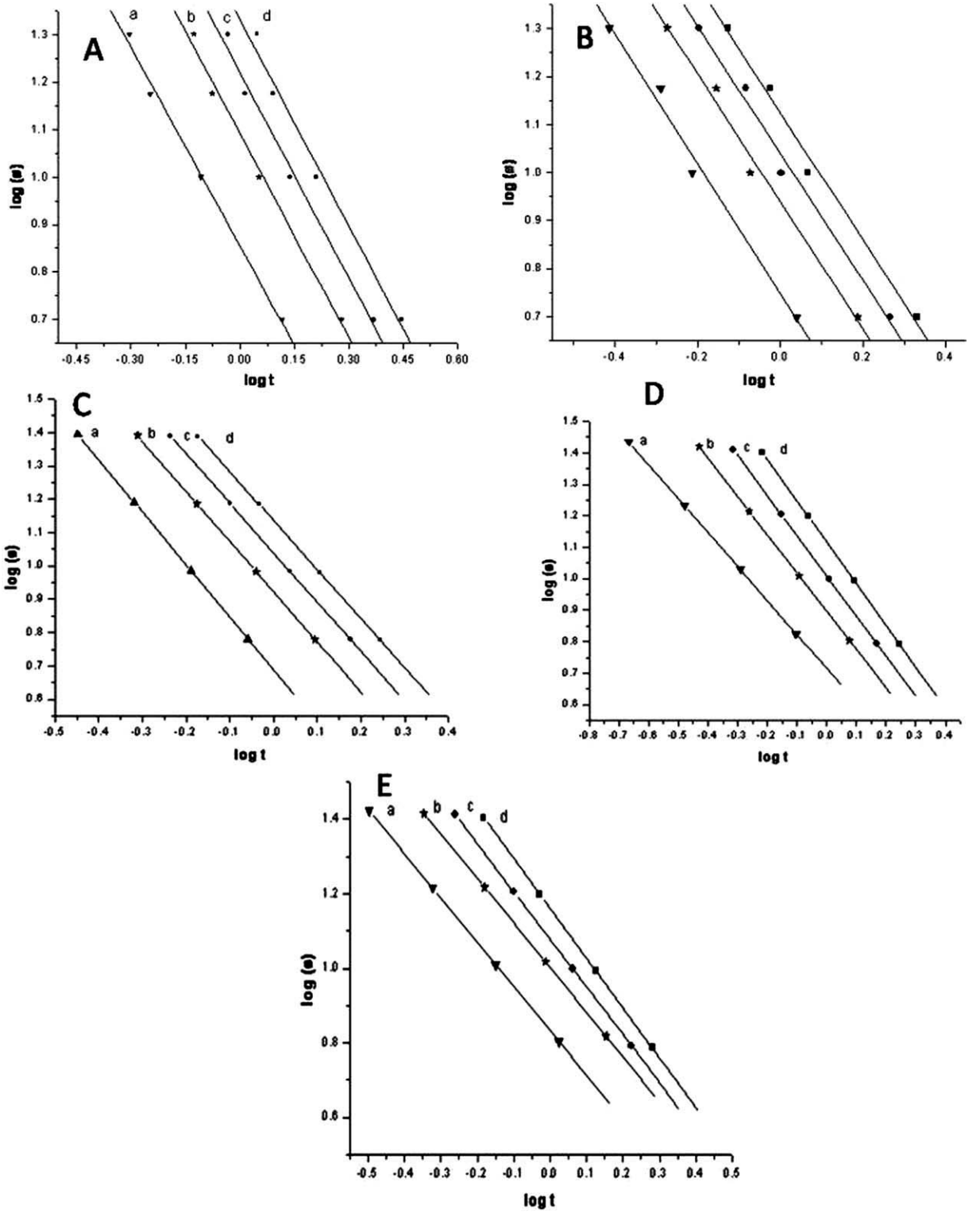

Figure 7. Plots of log φ versus log t for (A) PTT, (B) PTT/TiO_2, (C) PTT/GPS-grafted TiO_2, (D) PTT/PMMA-grafted TiO_2, and (E) PTT/amino-grafted TiO_2.

CONCLUSIONS

The influence of PTT/surface-treated TiO_2 nanoparticles with different groups on the crystallization behavior of PTT matrix has been evaluated. High degree of dispersion of the fillers in the final nanocomposites was prepared by melt-blending, PTT and surface-treated TiO_2 nanoparticles. The amino- and PMMA-grafted TiO_2 showed better miscibility within the PTT matrix. Avrami and Mo's methods were successful in describing

Table III. $F(T)$ and α Values of Mo's Method

	Φ (°C/min)	log $F(T)$	$F(T)$	α
PTT	5	0.85	7.08	1.39
	10	1.09	12.30	1.43
	15	1.22	16.59	1.45
	20	1.33	21.38	1.45
PTT/TiO_2	5	0.75	5.62	1.35
	10	0.94	8.71	1.33
	15	1.04	10.96	1.32
	20	1.13	13.49	1.32
PTT/GPS-grafted TiO_2	5	0.68	4.78	1.57
	10	0.92	8.32	1.51
	15	1.04	10.96	1.48
	20	1.14	13.80	1.47
PTT/PMMA-grafted TiO_2	5	0.72	5.24	1.08
	10	0.89	7.76	1.21
	15	1.01	10.23	1.27
	20	1.12	13.18	1.32
PTT/Amino-grafted TiO_2	5	0.83	6.76	1.19
	10	1.00	10.00	1.19
	15	1.07	11.75	1.28
	20	1.16	14.45	1.33

Table IV. Activation Energy by Kissinger Method Calculation

Materials	ΔE (kJ/mol)
Virgin PTT	169.18
PTT/TiO_2	221.69
PTT/GPS-grafted TiO_2	219.26
PTT/PMMA-grafted TiO_2	188.90
PTT/Amino-grafted TiO_2	199.43

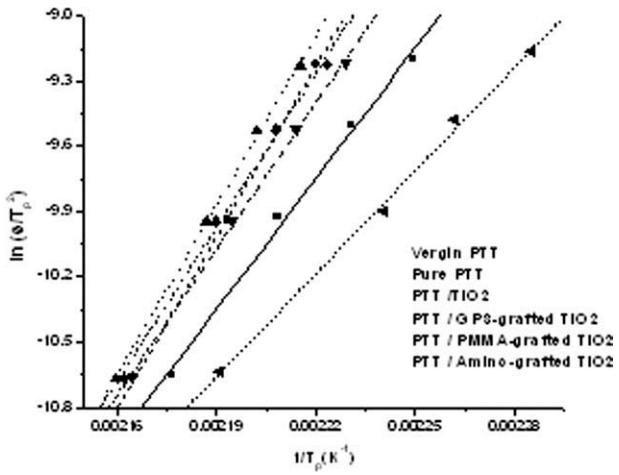

Figure 8. Plots of ln $[\varphi/T_p^2]$ vs. $1/T_p$ from the Kissinger method for nonisothermal crystallization activation energy of PTT/TiO_2 and surface-treated TiO_2 nanocomposites.

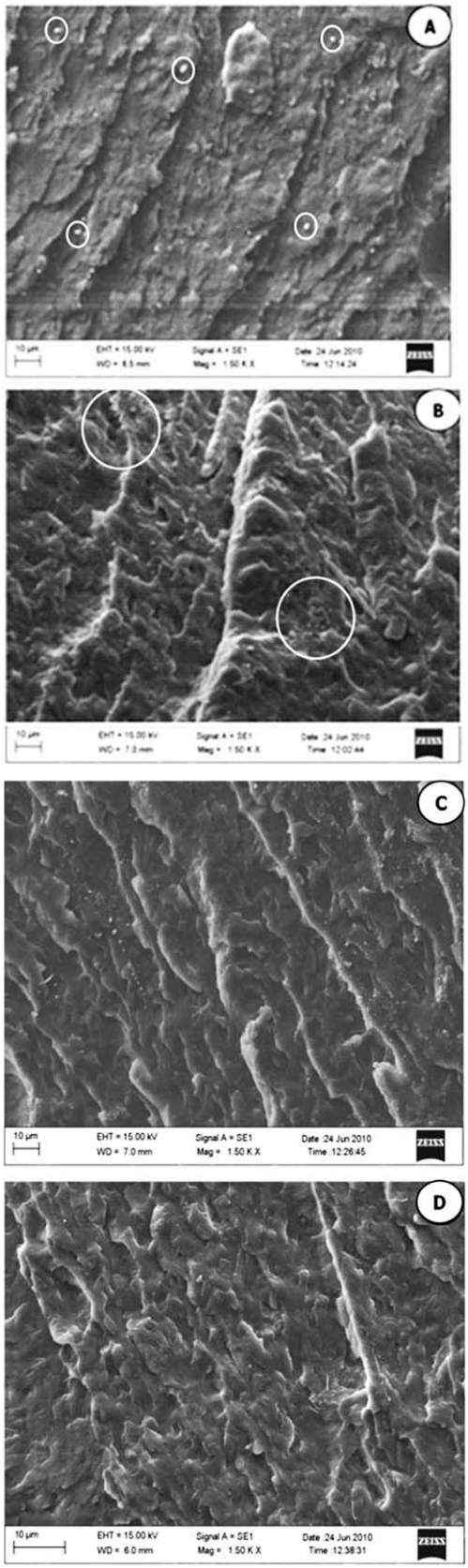

Figure 9. SEM microphotographs of (a) PTT/TiO_2, (b) PTT/GPS-grafted TiO_2, (c) PTT/PMMA-grafted TiO_2, and (d) amino-grafted TiO_2 nanocomposites.

the kinetics of the nonisothermal crystallization process. Addition of untreated TiO_2 and surface-treated TiO_2 into PTT matrix increased the crystallization temperature but decreased the crystallization rate of the nanocomposites. The GPS, PMMA, and amino-grafted TiO_2 samples show less degree of reduction in crystallization rate than the PTT/TiO_2 samples at a constant cooling rate because of the improved miscibility between the particles and the matrix improved. The crystallization time order obtained from the analysis methods is PTT $>$ TiO_2 $>$ GPS-grafted TiO_2 $>$ PMMA-grafted TiO_2 $\geq$ amino-grafted TiO_2 nanoparticles.

REFERENCES

1. Hasmukh, A. P.; Rajesh, S.; Hari, C. B.; Raksh, V. J. *Appl. Clay. Sci.* **2007,** *35*, 144.
2. Wang, Y.; Zhang, Q.; Fu, Q. *Macromol. Rapid. Commun.* **2003,** *24*, 231.
3. Li, Y. J.; Shimizu, H. *Macromol. Rapid. Commun.* **2005,** *26*, 710.
4. Chisholm, B. J.; Zimmer, J. G. *J. Appl. Polym. Sci.* **2000,** *76*, 1296.
5. Pyda, M.; Wunderlich, B. *J. Polym. Sci. Part B: Polym. Phys.* **2000,** *38*, 622.
6. Ward, I. M.; Wilding, M. A. *J. Polym. Sci. J. Polym. Phys.* **1976,** *14*, 263.
7. Yong, X. U.; Ye, S.-R.; Bian, J.; Oian, J.-W. *J. Mater. Sci.* **2004,** *39*, 5551.
8. Liu, Z.; Chen, K.; Yan, D. *J Polym Testing* **2004,** *23*, 323.
9. Huang, J. M.; Chang, F. C. *J. Polym. Sci. Part B: Polym. Phys.* **2000,** *38*, 934.
10. Ho, R. M.; Ke, K. Z.; Chen, M. *Macromolecules* **2000,** *33*, 7529.
11. Pyda, M.; Wunderlich, B. *J. Polym. Sci. Part B: Polym. Phys.* **2000,** *38*, 622.
12. Chung, W. T.; Yeh, W. J.; Hong, P. D. *J. Appl. Polym. Sci.* **2002,** *83*, 2426.
13. Hong, P. D.; Chung, W. T.; Hsu, C. F. *Polymer* **2002,** *43*, 3335.
14. Huang, J. M.; Chang, F. *J. Appl. Polym. Sci.* **2002,** *84*, 850.
15. Tsumashima, K.; Suzuki, M. Jpn. Pat. 08104763 (**1996**).
16. Zhang, Q.; Peng, H.; Zhang, Z. *J. Dispersion Sci. Technol.* **2007,** *28*, 937.
17. Kotek, J.; Kelnar, I.; Baldrian, J.; Raab, M. *Eur. Polym. J.* **2004,** *40*, 679.
18. Taniguchi, A.; Cakmak, M. *J. Polym.* **2004,** *45*, 6647.
19. Morawiec, J.; Pawlak, A.; Slouf, M.; Galeski, A.; Piorkowska, E.; Krasnikowa, N. *Eur. Polym. J.* **2005,** *41*, 1115.
20. Liu, Z.; Chen, K.; Yan, D. *Eur. Polym. J.* **2003,** *39*, 2359.
21. Lee, J. K.; Choi, M. J.; Eun Im, J.; Hwang, D. J.; Lee, K. H. *Polymer* **2007,** *48*, 2980.
22. Zhu, X.; Wang, B.; Chen, S.; Wang, C.; Zhang, Y.; Wang, H. *J. Macromol. Sci. Part B: Phys.* **2008,** *47*, 1117.
23. Run, M.; Yao, C.; Wang, Y. *Eur. Polym. J.* **2006,** *42*, 655.
24. Xu, Y.; Ye, S. *J. Mater. Sci.* **2004,** *39*, 5551.
25. Avella, M.; Bondioli, F.; Cannillo, V.; Pace, E. D.; Errico, M. E.; Ferrari, A. M.; Focher, B.; Malinconico, M. *Compos. Sci. Technol.* **2006,** *66*, 886.
26. Hong, P. D.; Chung, W. T.; Hsu, C. F. *Polymer.* **2002,** *43*, 3335.
27. Run, M.; Hao, Y.; Yao, C. *Thermochin. Acta.* **2009,** *495*, 51.
28. Avrami, M. *J. Chem. Phys.* **1939,** *7*, 1103.
29. Avrami, M. *J. Chem. Phys.* **1940,** *8*, 212.
30. Liu, Y.; Guo, W.; Su, Z.; Li, B.; Wu, C. *J. Macromol. Sci. Part B* **2009,** *48*, 414.
31. Liu, Z.; Chen, K.; Yan, D. *Eur. Polym. J.* **2003,** *39*, 2359.
32. Kong, X.; Yang, I.; Zhou, E.; Ma, D. *Eur. Polym. J.* **2000,** *36*, 1085.
33. Martins, J. C. A.; Novack, K. M.; Gomes, A. S. *Polymer.* **1998,** *39*, 6941.
34. Sajkiewicz, P.; Carpaneto, L.; Wasiak, A. *Polymer.* **2001,** *42*, 5365.
35. Rufina, G. A.; Brent, D. V.; Mandelkern, L. J. *Macromol.* **1995**, *28*, 3205.
36. Xu, W.; Ge, M.; He, P. J. *Appl. Polym. Sci.* **2001**, *82*, 2281.